EARTHQUAKE ENGINEERING AND STRUCTURAL DYNAMICS
Earthquake Engng Struct. Dyn. 2005; **34**:1489–1511
Published online 13 June 2005 in Wiley InterScience (www.interscience.wiley.com). DOI: 10.1002/eqe.495

Hysteretic models that incorporate strength and stiffness deterioration

Luis F. Ibarra[1,*,†,‡], Ricardo A. Medina[2] and Helmut Krawinkler[3]

[1]*Southwest Research Institute, CNWRA, San Antonio, TX 78238, U.S.A.*
[2]*Department of Civil and Environmental Engineering, University of Maryland, College Park, MD 20742, U.S.A.*
[3]*Department of Civil and Environmental Engineering, Stanford University, Palo Alto, CA 94305, U.S.A.*

SUMMARY

This paper presents the description, calibration and application of relatively simple hysteretic models that include strength and stiffness deterioration properties, features that are critical for demand predictions as a structural system approaches collapse. Three of the basic hysteretic models used in seismic demand evaluation are modified to include deterioration properties: bilinear, peak-oriented, and pinching. The modified models include most of the sources of deterioration: i.e. various modes of cyclic deterioration and softening of the post-yielding stiffness, and also account for a residual strength after deterioration. The models incorporate an energy-based deterioration parameter that controls four cyclic deterioration modes: basic strength, post-capping strength, unloading stiffness, and accelerated reloading stiffness deterioration. Calibration of the hysteretic models on steel, plywood, and reinforced-concrete components demonstrates that the proposed models are capable of simulating the main characteristics that influence deterioration. An application of a peak-oriented deterioration model in the seismic evaluation of single-degree-of-freedom (SDOF) systems is illustrated. The advantages of using deteriorating hysteretic models for obtaining the response of highly inelastic systems are discussed. Copyright © 2005 John Wiley & Sons, Ltd.

KEY WORDS: hysteretic behaviour; strength deterioration; cyclic deterioration; collapse

1. INTRODUCTION

The main objective of performance-based earthquake engineering is to evaluate the performance of a system at different seismic hazard levels. Considering the need for a comprehensive performance assessment, it becomes a necessity to develop hysteretic models that incorporate all-important phenomena contributing to demand prediction as the structure

*Correspondence to: Luis F. Ibarra, Southwest Research Institute, CNWRA, U.S.A.
†E-mail: libarra@swri.org
‡Senior Research Engineer.

Contract/grant sponsor: Pacific Earthquake Engineering Research (PEER) Center

Received 19 June 2004
Revised 12 January 2005
Accepted 1 March 2005

approaches collapse. In earthquake engineering, collapse implies that the structural system is no longer capable to maintain its gravity load-carrying capacity in the presence of seismic effects, which can be caused by main shocks and/or aftershocks. Local collapse may occur, for instance, if a vertical load-carrying component fails in compression or if shear transfer is lost between horizontal and vertical components (e.g. shear failure between a flat slab and a column). Global collapse occurs if a local failure propagates (progressive collapse) or if an individual storey displaces sufficiently so that the second order $P-\Delta$ effects fully offset the first order storey shear resistance. Collapse assessment requires hysteretic models capable of representing all the important modes of deterioration that are observed in experimental studies.

In most seismic demand studies, hysteresis models are being employed that have a non-deteriorating backbone curve and hysteresis rules that either ignore stiffness deterioration (bi-linear model) or account for stiffness deterioration by modifying the path with which the reloading branch approaches the backbone curve, e.g. the peak-oriented model [1] or various 'pinching' models. In 1970, Takeda [2] developed a model with a trilinear backbone curve that degrades the unloading stiffness based on the maximum displacement of the system. This model was created specifically for reinforced-concrete components, and the backbone curve is trilinear because it includes a segment for uncracked concrete. In addition to models with piecewise linear behaviour, smooth hysteretic models have been developed that include a continuous change of stiffness due to yielding, and sharp changes due to unloading, e.g. the Wen–Bouc model [3].

The need to simulate structural response far into the inelastic range, in which components deteriorate in strength and stiffness, led to the development of more versatile models such as the smooth hysteretic degrading model developed by Sivaselvan and Reinhorn [4], which includes rules for stiffness and strength deterioration as well as pinching. This model, however, does not include a negative backbone tangent stiffness. The model developed by Song and Pincheira [5] is capable of representing cyclic strength and stiffness deterioration based on dissipated hysteretic energy, and it is essentially a peak-oriented model that considers pinching based on deterioration parameters. The backbone curve includes a post-capping negative tangent stiffness and a residual strength branch. Because the backbone curve does not deteriorate, unloading and accelerated cyclic deterioration are the only modes included, and prior to reaching the peak strength the model is incapable of reproducing strength deterioration.

This paper has a threefold objective: (a) to describe the properties of proposed hysteretic models that incorporate both monotonic and cyclic deterioration; (b) to illustrate the calibration of these hysteretic models on component tests of steel, plywood, and reinforced-concrete specimens; and (c) to exemplify the utilization of the hysteretic models in the seismic response evaluation of single-degree-of-freedom (SDOF) systems.

2. PROPOSED HYSTERETIC MODELS INCLUDING STRENGTH AND STIFFNESS DETERIORATION

The need for improved analytical models in seismic demand evaluation studies is evident from Figure 1, which shows a monotonic load–displacement response and a superimposed quasi-static cyclic response of 'identical' plywood shear wall panels [6]. The monotonic test result shows that strength is 'capped' and is followed by a negative tangent stiffness. The cyclic hysteretic response indicates that strength deteriorates with the number and amplitude

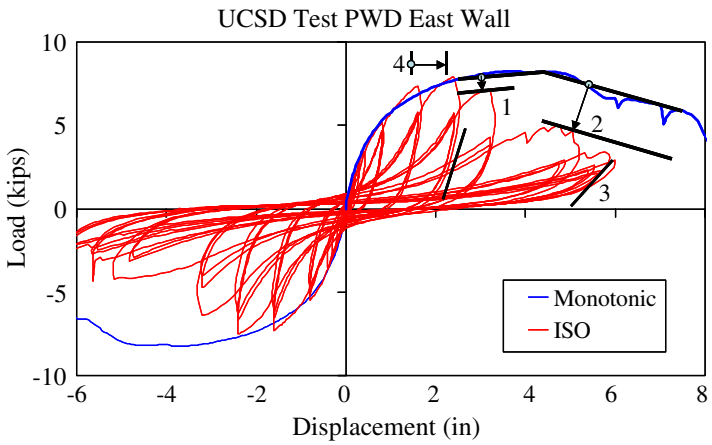

Figure 1. Monotonic and cyclic experimental response of a plywood panel [6].

of cycles, even if the displacement associated with the strength cap has not been reached (1). It also indicates that strength deterioration occurs in the post-capping range (2), and that the unloading stiffness may also deteriorate (3). Furthermore, it is observed that the reloading stiffness may deteriorate at an accelerated rate (4).

Several hysteretic models have been developed to represent hysteretic behaviour similar to that of Figure 1 [4, 5]. However, few models integrate all the important deterioration sources such as strength deterioration in the backbone curve (post-capping stiffness branch) and cyclic deterioration of strength and stiffness. For this reason, deteriorating models are developed in this study for bilinear, peak-oriented and pinched hysteretic systems. The models are implemented in an in-house computer program called SNAP, which is based on the program NLDYNA [7]. SNAP is used to carry out dynamic and quasi-static inelastic analysis of SDOF systems. The component deterioration models are also implemented in the computer program DRAIN-2DX [8], which is used to carry out dynamic non-linear analyses of multi-degree-of-freedom (MDOF) systems.

This section presents a description of the salient properties of the proposed deteriorating hysteretic models. In the discussion the term deteriorating hysteretic models refers to models that include strength deterioration of the backbone curve and/or cyclic deterioration. Conversely, non-deteriorating hysteretic models do not incorporate any of the above types of deterioration.

2.1. *Backbone curve*

The backbone curve defines the monotonically increasing deformation response for all the hysteretic models considered in this paper (Figure 2). If no deterioration exists, the backbone curve is defined by three parameters: the elastic (initial) stiffness K_e, the yield strength F_y, and the strain-hardening stiffness $K_s = \alpha_s K_e$. If deterioration of the backbone curve is included, a softening branch begins at the cap deformation (δ_c), which corresponds to the peak strength (F_c) of the load–deformation curve. If δ_c is normalized by the yield deformation, the resulting

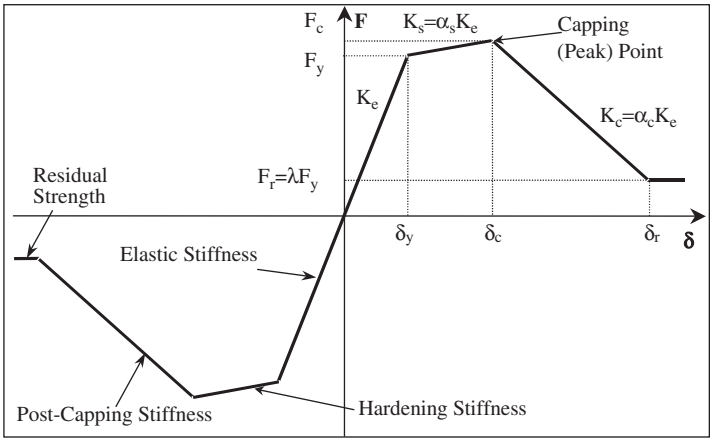

Figure 2. Backbone curve for hysteretic models.

ratio may be denoted as ductility capacity[§] (δ_c/δ_y). The softening branch is defined by the post-capping stiffness, $K_c = \alpha_c K_e$, which usually has a negative value. In addition, a residual strength can be assigned to the model, $F_r = \lambda F_y$, which represents the fraction of the yield strength of the component that is preserved once a given deterioration threshold is achieved. When such a residual strength is specified, the backbone curve is supplemented with a horizontal line of ordinate F_r, and the strength will not drop below this value, i.e. the residual strength is not modified when cyclic deterioration shrinks the backbone curve.

The parameters α_s, δ_c/δ_y, α_c, and λ are obtained either from analytical predictions or from calibration of the hysteretic models with load–deformation data obtained from experiments. The hysteretic models allow these parameters to have different values in the positive and negative directions.

2.2. *Description of hysteretic models without cyclic deterioration*

This section describes the modifications to traditional hysteretic models needed to incorporate the deteriorating backbone curve of Section 2.1. The cyclic deterioration rules that can be applied to all the models are introduced in Section 2.3.

2.2.1. Bilinear model[¶]. This model is based on the standard bilinear hysteretic rules with kinematic strain hardening. These basic rules are preserved once post-capping and residual strength branches are included. However, it is necessary to introduce the 'strength limit' shown in Figure 3 when the backbone curve includes a branch with negative slope. According to kinematic rules, the loading segment that starts at point 5 should continue up to intersect

[§]Traditionally, the term 'ductility' refers to the ability of a component or a system to displace inelastically without significant deterioration in strength or stiffness. In this research, 'ductility capacity' is defined at the component level as the ratio of the deformation at peak strength to the yield deformation.

[¶]The term 'bilinear hysteretic model' is used to define a hysteretic model with kinematic strain hardening, and it does not refer to the number of segments used to model the backbone curve.

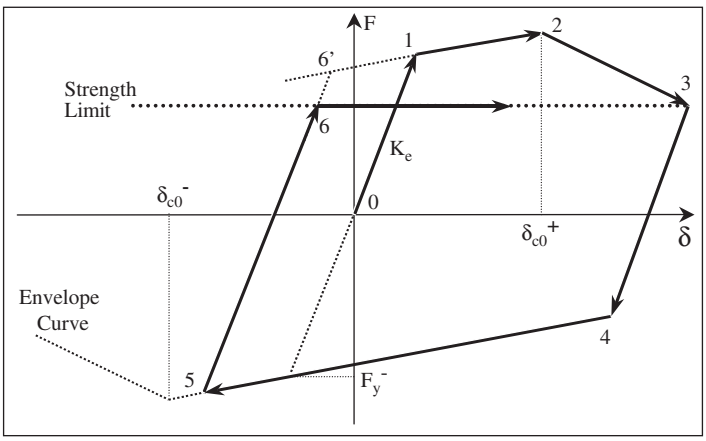

Figure 3. Bilinear hysteretic model with strength limit.

point 6′. However, this loading segment ends when it intersects the 'strength limit' at point 6. The limit corresponds to the strength of point 3, which is the smallest strength in the non-linear range of the backbone curve in earlier cycles. If this condition were not established, the strength in the loading path could increase in later stages of deterioration.

2.2.2. Peak-oriented model. This model keeps the basic hysteretic rules proposed by Clough and Johnston [1] and later modified by Mahin and Bertero [9], but the backbone curve is modified to include strength capping and residual strength. The presence of a negative post-capping stiffness does not modify any basic rule of the model. Figure 4 shows the deterioration of the reloading stiffness for a peak-oriented model once the horizontal axis is reached (points 3, 7, and 11). The reloading path always targets the previous maximum displacement, except when the Mahin and Bertero modification applies [9].

2.2.3. Pinching model. The pinching model is similar to the peak-oriented one, except that reloading consists of two parts. Initially the reloading path is directed towards a 'break point', which is a function of the maximum permanent deformation and the maximum load experienced in the direction of loading. The break point is defined by the parameter κ_f, which modifies the maximum 'pinched' strength (points 4 and 8 of Figure 5(a)), and κ_d, which defines the displacement of the break point (points 4′ and 8′). The first part of the reloading branch is defined by $K_{rel,a}$ and once the break point is reached (points 4′ and 8′), the reloading path is directed towards the maximum deformation of earlier cycles in the direction of loading ($K_{rel,b}$).

If the absolute deformation at reloading (point 13, Figure 5(b)) is larger than the absolute value of $(1 - \kappa_d)\delta_{per}$, the reloading path consists of a single branch that is directed towards the previous maximum deformation in the direction of loading.

2.3. Cyclic strength and stiffness deterioration based on hysteretic energy dissipation

Four cyclic deterioration modes may be activated once the yield point is surpassed in at least one direction: basic strength, post-capping strength, unloading stiffness, and reloading stiffness

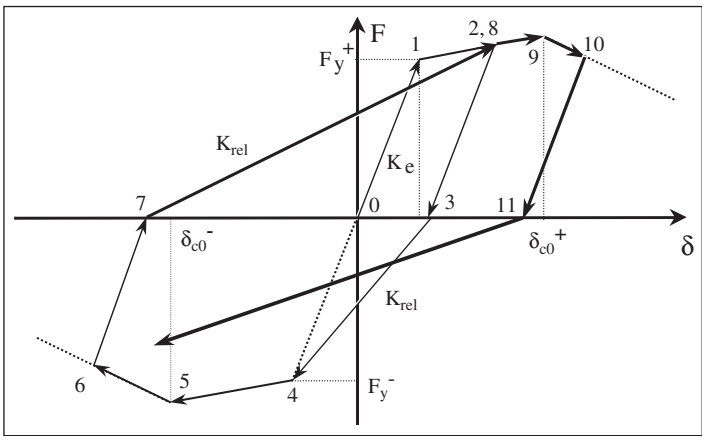

Figure 4. Basic rules for peak-oriented hysteretic model.

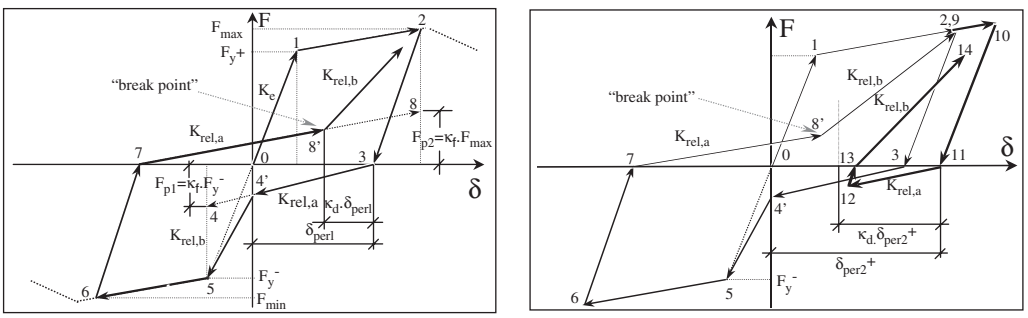

Figure 5. Pinching hysteretic model: (a) basic model rules; and (b) modification if reloading deformation is to the right of break point.

deterioration. The cyclic deterioration rules are the same for all the hysteretic models with the exception of the accelerated stiffness deterioration, which does not exist in the bilinear model. The peak-oriented model will be used to illustrate the effect of cyclic deterioration.

The cyclic deterioration rates are controlled by the rule developed by Rahnama and Krawinkler [7], which is based on the hysteretic energy dissipated when the component is subjected to cyclic loading. It is assumed that every component possesses a reference inherent hysteretic energy dissipation capacity, regardless of the loading history applied to the component (see Section 5 for more details).

The cyclic deterioration in excursion i is defined by the parameter β_i, which is given by the following expression:

$$\beta_i = \left(\frac{E_i}{E_t - \sum_{j=1}^{i} E_j} \right)^c \tag{1}$$

E_i is the hysteretic energy dissipated in excursion i, ΣE_j the hysteretic energy dissipated in all previous excursions through loading in both positive and negative directions, E_t the reference hysteretic energy dissipation capacity, $E_t = \gamma F_y \delta_y$. The parameter γ expresses the hysteretic energy dissipation capacity as a function of twice the elastic strain energy at yielding ($F_y \delta_y$), it is calibrated from experimental results and can be different for each deterioration mode. Finally, c is the exponent defining the rate of deterioration. Rahnama and Krawinkler [7] suggest that a reasonable range for c is between 1.0 and 2.0. If the displacement history consists of constant amplitude cycles, a unit value for c implies an almost constant rate of deterioration. For the same displacement history, a value $c = 2$ slows down the rate of deterioration in early cycles and accelerates the rate of deterioration in later cycles [7].

Throughout the loading history, β_i must be within the limits $0 < \beta_i \leqslant 1$. If β_i is outside these limits ($\beta_i \leqslant 0$ or $\beta_i > 1$), the hysteretic energy capacity is exhausted and collapse is assumed to take place. Mathematically,

$$\gamma F_y \delta_y - \sum_{j=1}^{i} E_j < E_i \tag{2}$$

The individual modes of deterioration are described below.

2.3.1. Basic strength deterioration. It is defined by translating the strain hardening branch toward the origin by an amount equivalent to reducing the yield strength to

$$F_i^+ = (1 - \beta_{s,i}) F_{i-1}^+ \quad \text{and} \quad F_i^- = (1 - \beta_{s,i}) F_{i-1}^- \tag{3}$$

$F_i^{+/-}$ and $F_{i-1}^{+/-}$ are the deteriorated yield strength after and before excursion i respectively.

There is a positive and a negative value for each deterioration parameter because the algorithm deteriorates the strength independently in both directions. That is to say, F_i^- is updated after every positive inelastic excursion, and F_i^+ is updated after every negative inelastic excursion.

The parameter $\beta_{s,i}$ is calculated with Equation (1) each time the inelastic path crosses the horizontal axis and is associated with the appropriate γ value to model basic strength deterioration (γ_s).

The basic strength deterioration mode also includes the deterioration of the strain hardening slope, which is rotated in accordance with the following equation:

$$K_{s,i}^+ = (1 - \beta_{s,i}) K_{s,i-1}^+ \quad \text{and} \quad K_{s,i}^- = (1 - \beta_{s,i}) K_{s,i-1}^- \tag{4}$$

The strain hardening slope is also deteriorated independently in both directions. The consequence is that the slope of the strain hardening branch is equal to zero when the yield strength has deteriorated to zero. If a residual branch is included in the backbone curve, the analytical model deteriorates the strain-hardening stiffness to zero ($K_{s,i}^{+/-} = 0$) when the yield strength deteriorates to λF_{y0} (F_{y0} is the initial yield strength).

A peak-oriented model is used in Figure 6(a) to illustrate the basic strength deterioration mode. At point 3, β_s is calculated for first time and the yield strength on the negative side is reduced from F_y^- to F_1^-. In addition, the slope of the hardening branch decreases from $K_{s,0}^-$ to $K_{s,1}^-$. At point 7, β_s is calculated again and the positive yield strength is modified from F_y^+ to F_1^+. Observe that the current β_s value is used to modify only the strength in the

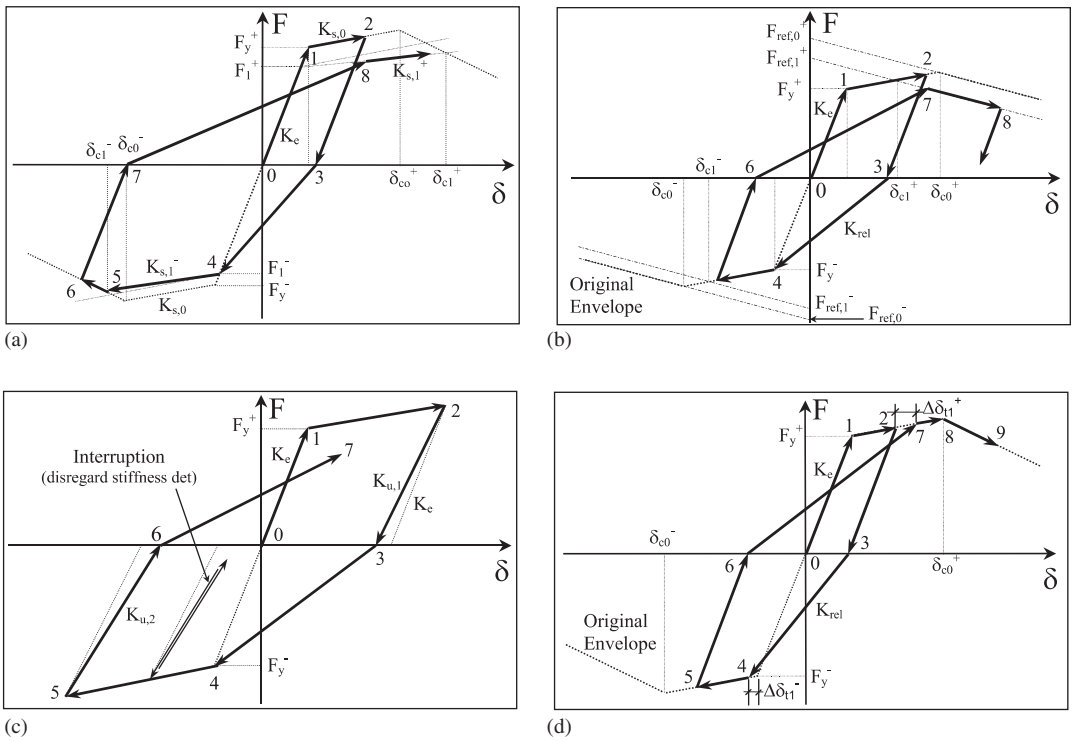

Figure 6. Individual deterioration modes, illustrated on a peak-oriented model: (a) basic strength deterioration; (b) post-capping strength deterioration; (c) unloading stiffness deterioration; and (d) accelerated reloading stiffness deterioration.

current loading direction, based on the previous strength in that direction, i.e. the strength in the opposite direction is not modified.

2.3.2. Post-capping strength deterioration. This deterioration mode, illustrated in Figure 6(b), translates the post-capping branch towards the origin and, unlike basic strength deterioration, the slope of the post-capping branch is kept constant. The post-capping branch is moved inwards by an amount equivalent to reducing the reference strength according to the following equation:

$$F_{ref,i}^{+/-} = (1 - \beta_{c,i}) F_{ref,i-1}^{+/-} \tag{5}$$

$F_{ref}^{+/-}$ is the intersection of the vertical axis with the projection of the post-capping branch (Figure 6(b)). There is a positive and negative reference strength parameter for independently deteriorating the positive and negative post-capping strength. The parameter β_c is calculated with Equation (1) and is associated with an appropriate γ value to model post-capping strength deterioration (γ_c).

The deterioration of post-capping strength is computed each time the horizontal axis is crossed, but it may not affect the loading path in early stages of non-linearity. In Figure 6(b) the first post-capping strength deterioration is calculated at point 3 and the negative reference point moves to $F^{-}_{ref,1}$. This backbone modification does not affect the loading path because the negative displacement does not reach the post-capping branch. At point 6, the post-capping strength deterioration is computed again, and this time the loading path is modified because the updated cap displacement ($\delta^{+}_{c,1}$) is exceeded in this excursion.

2.3.3. Unloading stiffness deterioration. The unloading stiffness (K_u) is deteriorated in accordance with the following equation:

$$K_{u,i} = (1 - \beta_{k,i}) K_{u,i-1} \tag{6}$$

$K_{u,i}$ and $K_{u,i-1}$ are the deteriorated unloading stiffnesses after and before excursion i, respectively. The parameter $\beta_{k,i}$ is computed from Equation (1) and is associated with an appropriate cyclic deterioration parameter γ_k. It is the only β-parameter that is computed when a load reversal takes place in the inelastic range, unlike the other three β-parameters that are computed when the loading path crosses the horizontal axis. Furthermore, this is the only deterioration mode in which the deteriorating quantity, i.e. the unloading stiffness, is updated simultaneously in both directions (i.e. for positive and negative unloading). Consequently, the unloading stiffness deteriorates up to twice as much as the other deteriorating quantities, and if the same rate of deterioration is expected in the four deterioration modes, γ_k should be about twice as large as the other γ values, i.e. $\gamma_k = 2\gamma_{s,c,a}$.

Figure 6(c) shows a peak-oriented model that includes unloading stiffness deterioration. At point 2 the first reversal in the inelastic range occurs and the unloading stiffness deteriorates from K_e to $K_{u,1}$. At point 5 the first reversal on the negative side takes place and $K_{u,2}$ is calculated based on the updated β_k and $K_{u,1}$. Unlike other deterioration modes, $K_{u,2}$ is updated based on the value of the unloading stiffness on the other side of the loop.

Unloading stiffness deterioration is disregarded if the reversal is considered an interruption in the direction of loading. In peak-oriented and pinching models, an interruption occurs when the path is on the unloading stiffness and a reversal takes place before the path targets the maximum displacement on the opposite side (see Figure 6(c)). In the bilinear model, an interruption occurs when the path is on the unloading stiffness and has a reversal before reaching the backbone curve on the opposite side.

2.3.4. Accelerated reloading stiffness deterioration. This deterioration mode increases the absolute value of the target displacement, defined as the maximum positive or negative displacement of past cycles, according to the direction of loading. Accelerated reloading stiffness deterioration is defined only for peak-oriented and pinching models, and it is governed by the following equation:

$$\delta^{+/-}_{t,i} = (1 + \beta_{a,i}) \delta^{+/-}_{t,i-1} \tag{7}$$

There is a target displacement (δ_t) for each loading direction, and the reloading stiffness deterioration is calculated each time the horizontal axis is crossed (Figure 6(d)). Equation (1) is employed to compute β_a based on an appropriate parameter γ_a.

3. CALIBRATION OF HYSTERETIC MODELS ON COMPONENT TESTS

The deteriorating hysteretic models have been calibrated with load–deformation data obtained from experiments on steel, plywood, and reinforced-concrete components. Simulations are obtained by tuning the deterioration parameters to experimental data.

3.1. Steel specimens

Figures 7(a) and (b) illustrate the calibration of the bilinear model on beam load–displacement relationships for steel beam-column subassemblies [10]. Because monotonic tests were not available to obtain the backbone curve for the simulations, the parameters of the backbone curve (F_y, δ_y, δ_c, α_s and α_c) were estimated from the load–displacement relationship of the

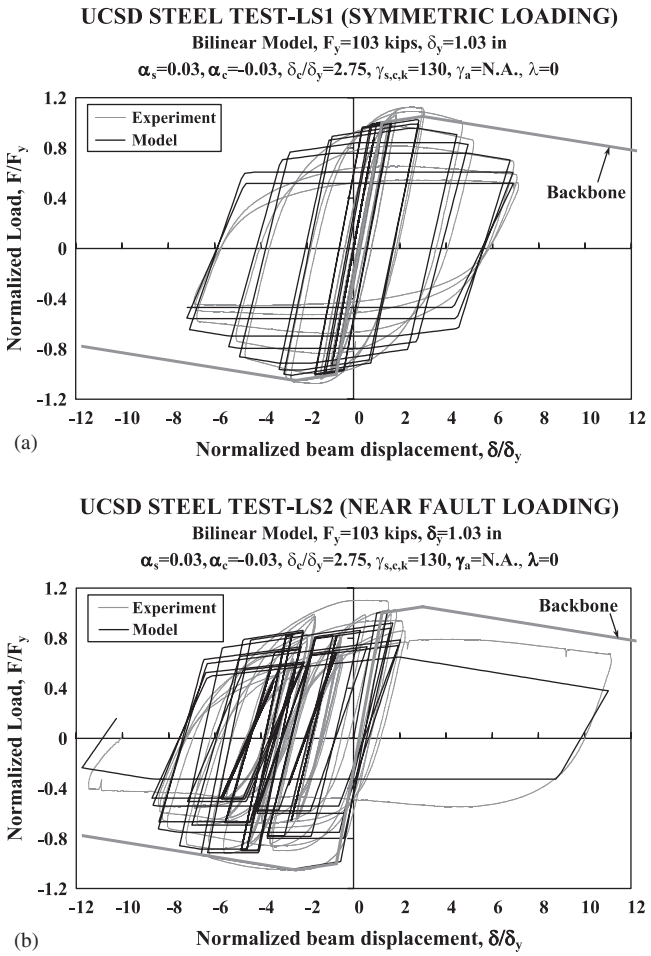

Figure 7. Calibration of bilinear model on steel component tests [10]: (a) test LS-1, SAC standard loading protocol; and (b) test LS-2, SAC near-fault protocol.

second excursion of the near-fault test (Figure 7(b)). This second excursion is considered to be close to a monotonic load–displacement relationship because only small structural damage occurred during the first excursion in the opposite direction. Based on this approach, the following properties are utilized for the simulations: $F_y = 103$ kips, $\delta_y = 1.03$ in, $\alpha_s = 0.03$, $\alpha_c = -0.03$, $\delta_c/\delta_y = 2.75$ and no residual strength ($\lambda = 0$). The cyclic deterioration parameters are: $c = 1.0$ and $\gamma_s = \gamma_c = \gamma_k = 130$. The use of different γ values for each deterioration mode could have resulted in a somewhat better calibration. However, all γ's are set at the same value to illustrate that adequate simulations can be obtained through the use of a single hysteretic energy dissipation parameter. It turns out that the response is not very sensitive to small variations in γ's. An appropriate value was obtained by a trial and error method that provided an empirical best fit to the experimental data.

The two specimens, LS-1 and LS-2, are identical but are subjected to very different loading histories, which provides an opportunity to assess the generality of a deterioration model that includes cyclic deterioration. The analytical model provides a reasonable correlation with the experimental loops for both loading histories, within the constraints of a simple bilinear model that does not account for cyclic hardening, a phenomenon that may lead to a considerable increase in strength during early cycles in which little cyclic deterioration is noticeable. The important observation is that the large inelastic cycles, in which significant cyclic deterioration takes place, are well simulated by the analytical model.

Figure 8 shows plots of negative and positive normalized hysteretic energy (NHE = hysteretic energy dissipated/$F_y\delta_y$) as a function of the number of cycles for the two specimens. In all cases the history of NHE is similar for both the analytical model and the experimental results. Thus, the bilinear hysteretic model is able to replicate the cumulative energy dissipated under the action of various loading protocols.

Note that the sum of positive and negative NHE is smaller than the input parameter $\gamma_{s,c,k} = 130$. The reasons are that (a) complete loss of restoring force is not reached in either case, and (b) deterioration in these examples comes to a large part from cyclic loading but in part also from the presence of a post-capping stiffness which does not depend on NHE. A reasonable calibration of the hysteretic model refers to the selection of model parameters that produce NHE histories that are close to those exhibited in the component tests throughout the entire range of loading. The fact that the NHE at the end of loading does not correspond with the $\gamma_{s,c,k,a}$ value does not imply that the selected cyclic deterioration parameters are erroneous.

3.2. *Plywood specimens*

Figure 9 shows the calibration of the pinching model based on plywood shear wall test results [6]. Four 'identical' specimens were subjected to different loading protocols. The problem with plywood panels is that 'identical' specimens cannot be created because of differences in workmanship, and response differences have to be expected even if identical loading histories are applied. This is evident from the backbone curve, which is obtained from a monotonic test but is clearly exceeded in two of the four cyclic test results illustrated in Figure 9. Nevertheless, the responses to the very different loading histories permit a general assessment of the adequacy of the proposed deterioration models. In particular, the SPD loading protocol, see Figure 9(c), has a very large number of cycles that causes a very different response from those of the other three loading histories. The proposed deterioration model,

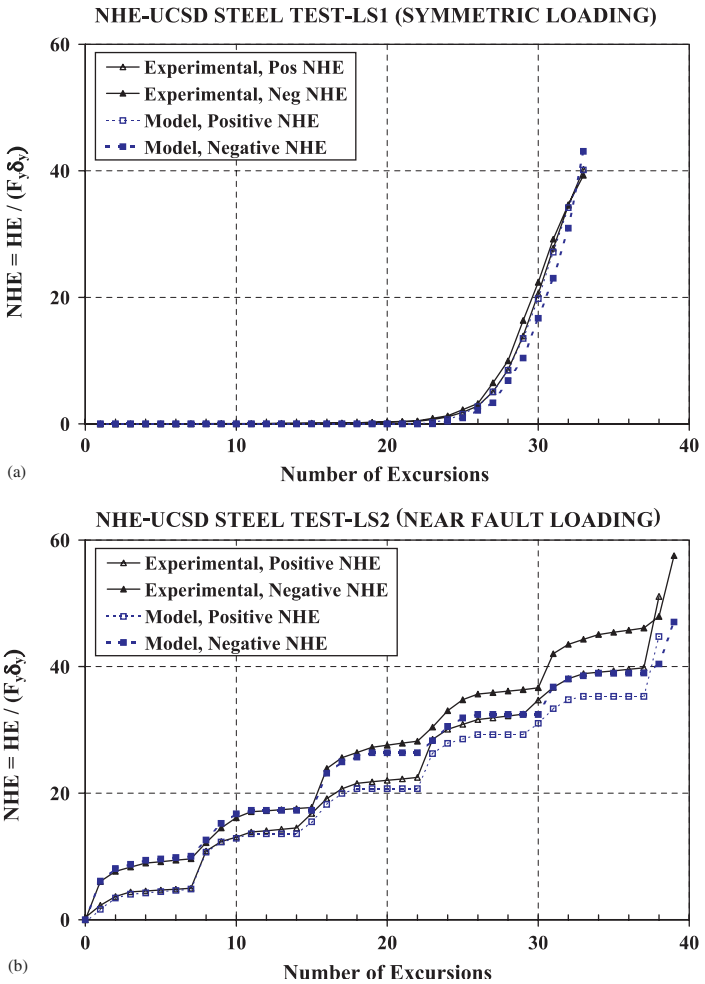

Figure 8. History of NHE dissipation, tests of Figure 7: (a) Test LS-1, SAC standard loading protocol; and (b) test LS-2, SAC near-fault protocol.

with the parameters shown in the figures, seems to be capable of simulating the effect of the many cycles.

Figure 10 shows plots of positive and negative NHE as a function of the number of cycles. In all cases, the history of the NHE of the analytical model is below the one corresponding to the experimental results because the model remains elastic until δ_y is attained. That is to say, the models do not dissipate energy below this threshold whereas the experimental results exhibit energy dissipation at displacement levels well below the estimated value of δ_y. Although the trends in the history of NHE between the model and test results are slightly offset by this difference, the pinching model is able to replicate the cumulative energy dissipated, especially at relatively large deformation levels.

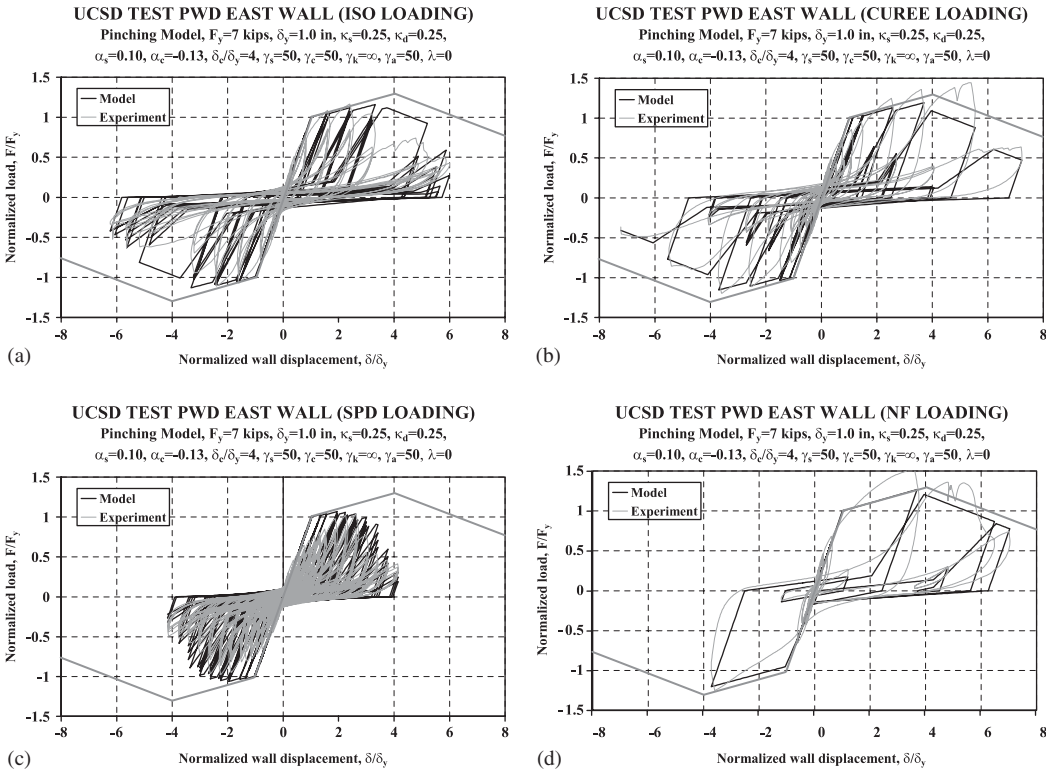

Figure 9. Calibration of pinching model on plywood shear-wall component tests [6]: (a) ISO loading protocol; (b) CUREE standard loading protocol; (c) SPD loading protocol; and (d) CUREE near-fault loading protocol.

It is noted that the total NHE (positive and negative) of Figure 10(c) is close to the γ value of 50 selected for the analytical model, whereas that of Figure 10(d) is only about 13. The reason is that in the SPD loading protocol test the specimen loses most of its resistance because of cyclic deterioration, whereas in the CUREE near-fault loading protocol test the specimen loses much of its resistance because of the presence of a post-capping stiffness.

3.3. Reinforced-concrete specimens

The calibration of reinforced-concrete specimens utilizes experiments carried out by Sezen [11]. Sezen tested columns with deficient transverse reinforcement, which were connected to very rigid top and base beams to produce double curvature bending. The two columns with small constant axial load $P = 0.15 f'_c A_g$ are used for calibration. One column was subjected to a stepwise increasing cyclic loading protocol and the other column to a mostly monotonic history, consisting of several small cycles followed by a large monotonic excursion. For calibration purposes, the backbone parameters were based on the results of the second column test. Figure 11 presents the experimental and analytical hysteretic loops of the cyclic loading test along with the model parameters. The figure exemplifies the difficulties in reproducing

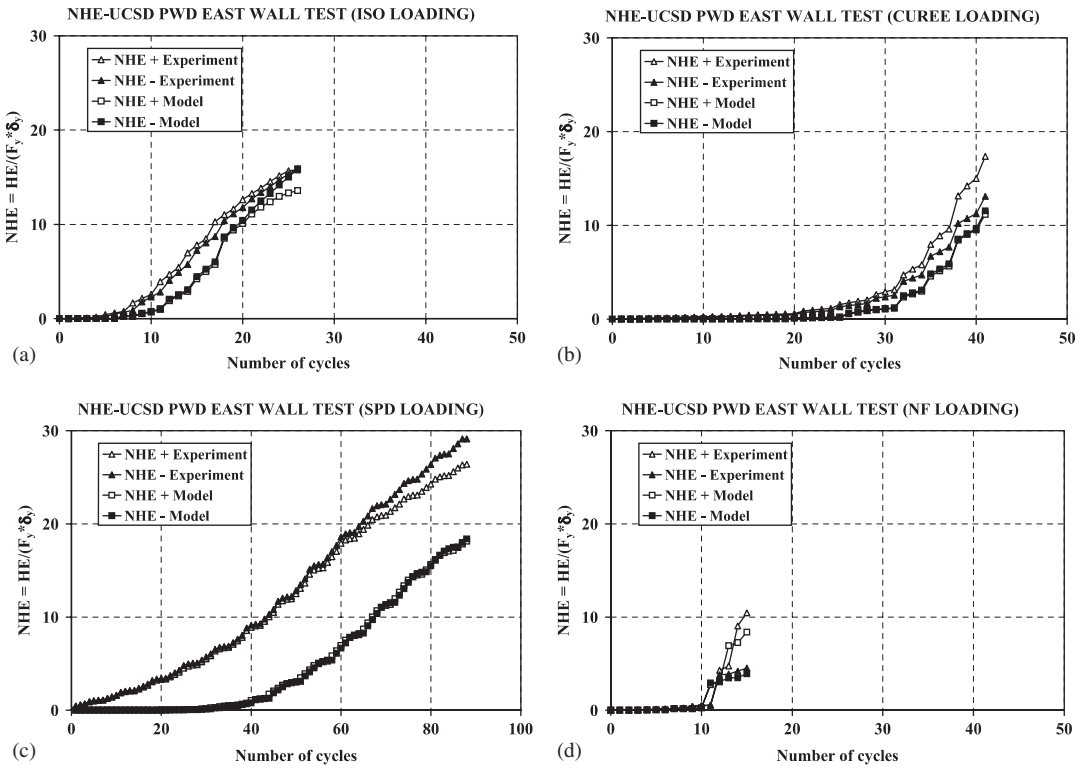

Figure 10. History of NHE dissipation, tests of Figure 9: (a) ISO loading protocol; (b) CUREE standard loading protocol; (c) SPD loading protocol; and (d) CUREE near-fault loading protocol.

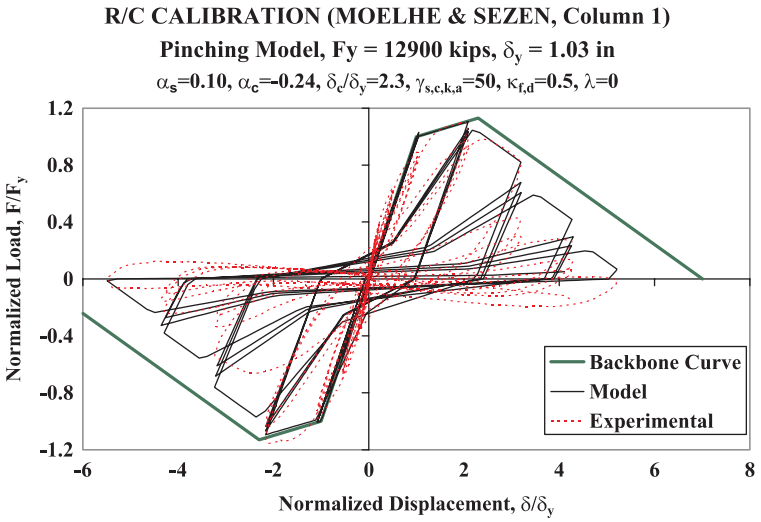

Figure 11. Calibration of pinching model on a reinforced-concrete column [11].

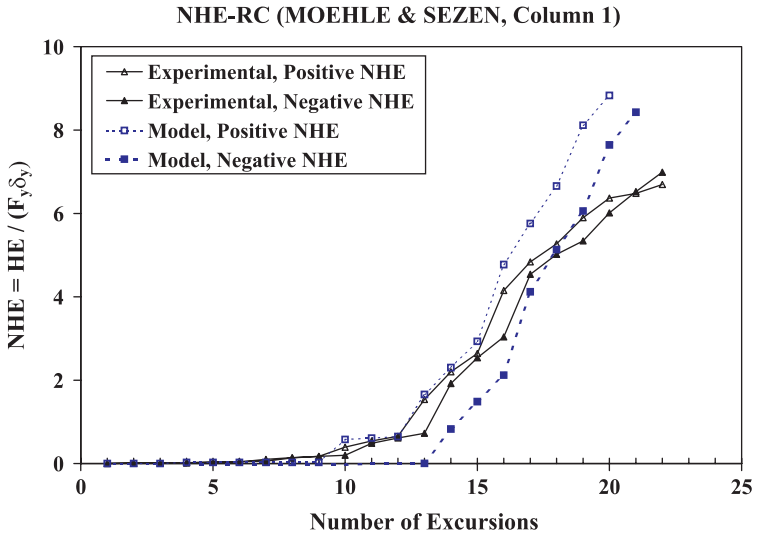

Figure 12. History of NHE dissipation, test of Figure 11.

early inelastic cycles in reinforced-concrete components when the analytical model does not include the cracking point. However, the deteriorating pinching model simulates well the highly inelastic behaviour.

Figure 12 depicts the NHE dissipation histories for the case shown in Figure 11. The sum of positive and negative NHE is small compared to $\gamma = 50$. The reason is that much of the deterioration is caused by the presence of a negative post-capping tangent stiffness rather than by cyclic deterioration effects.

4. ILLUSTRATIONS OF CYCLIC DETERIORATION EFFECTS

Figures 14 and 15 illustrate the effect of ductility capacity, post-capping stiffness, and cyclic deterioration on the hysteretic response of a component subjected to the CUREE loading protocol [12], which is shown in Figure 13.

Figure 14 shows four hysteretic responses with common post-capping stiffness, $\alpha_c = -0.10$. From left to right of the figure, the ductility capacity decreases from $\delta_c/\delta_y = 6$ to $\delta_c/\delta_y = 2$, whereas from top to bottom of the figure the cyclic deterioration parameter decreases from $\gamma_{s,c,k,a} =$ Infinite to $\gamma_{s,c,k,a} = 25$. There are clear patterns both in the horizontal and vertical directions for this specific loading history. For instance, the ductility capacity becomes unimportant if the cyclic deterioration parameter is very small ($\gamma_{s,c,k,a} = 25$), i.e. cyclic deterioration effects overpower the effect of monotonic ductility, see bottom row of Figure 14. This is a consistent but not very important observation, because the combination of a monotonically ductile component that experiences rapid cyclic deterioration is unlikely. For the rest of the cases, the combination of ductility capacity and cyclic deterioration parameters control the response.

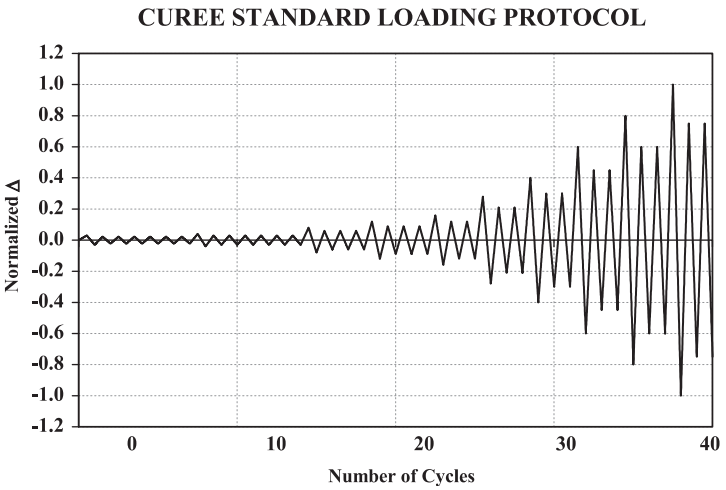

Figure 13. CUREE standard loading protocol.

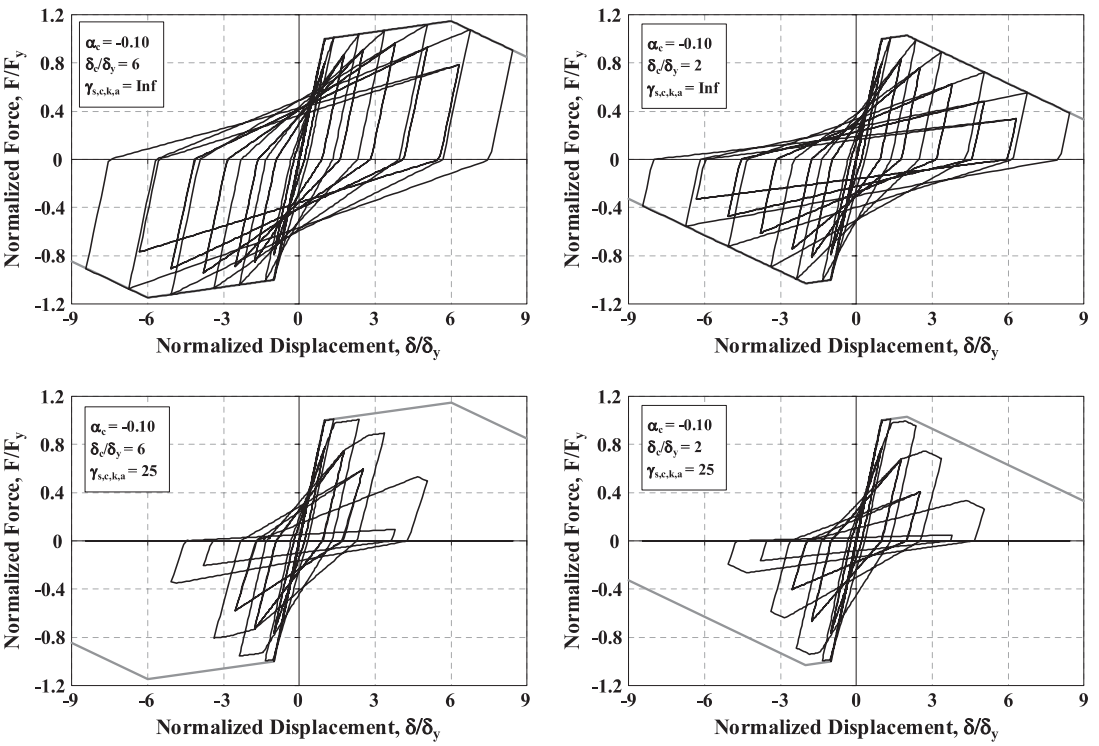

Figure 14. Effects of deterioration on hysteretic response; peak-oriented model, CUREE protocol, $\alpha_s = 0.03$, $\alpha_c = -0.10$.

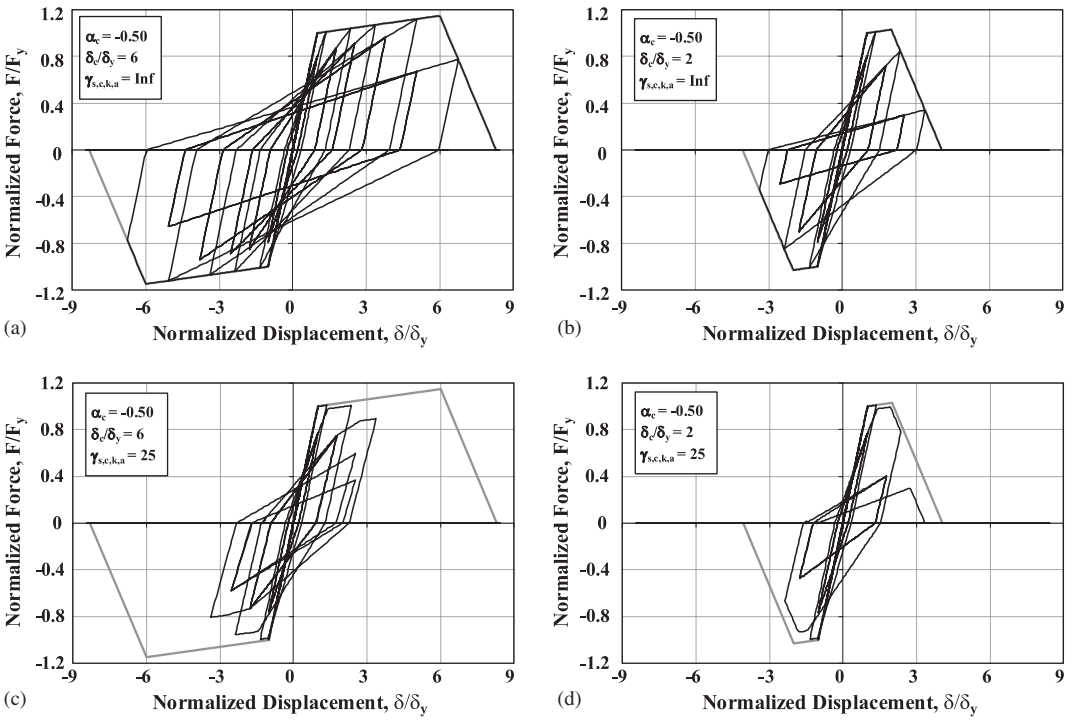

Figure 15. Effects of deterioration on hysteretic response; peak-oriented model, CUREE protocol, $\alpha_s = 0.03$, $\alpha_c = -0.50$.

Figure 15 presents the same arrangement of systems, but using a steeper post-capping slope $\alpha_c = -0.50$. The large differences between Figures 14 and 15 demonstrate the importance of the post-capping stiffness. For $\alpha_c = -0.50$ the monotonic ductility capacity becomes very important because little 'life' is left at deformations exceeding the monotonic ductility capacity.

In summary, the deterioration effects of individual parameters cannot be isolated. The cyclic behaviour is governed by the combination of all three of the parameters varied in Figures 14 and 15 (δ_c/δ_y, α_c, $\gamma_{s,c,k,a}$).

5. ADDITIONAL OBSERVATIONS ON DETERIORATION MODEL

The main advantage of the proposed deterioration model is its versatility, which makes it feasible to represent many deterioration modes in a transparent manner utilizing physical parameters that can be deduced from experimental results. The cyclic deterioration modes may be expressed by a single parameter ($\gamma_{s,c,k,a}$), if it is acceptable that all cyclic deterioration modes can be approximated by the same γ value, and that the exponent in Equation (1) can be taken as 1.0. There is no simpler way to describe cyclic deterioration. It is the combination of this single cyclic deterioration parameter with a backbone curve incorporating a negative

post-capping tangent stiffness that makes this deterioration model simple but versatile. The following observations are made in the context of damage and deterioration modelling.

- There are fundamental differences between the proposed deterioration model and cumulative damage models. The latter count cumulative damage and use a counter (often referred to as a damage index) to indicate the degree of damage or complete 'failure' (for the latter the counter usually takes a value of 1.0). Most cumulative damage models (e.g. the Park–Ang model [13]) do not consider the fact that cumulative damage causes a decrease in strength and stiffness of components and therefore lead to an increase in deformations in a structure, which ultimately may cause collapse. The component cumulative damage models known to the authors do not permit tracking of the response of a structure till collapse, whereas the component deterioration models proposed here, when implemented in a computer analysis program, do permit prediction of collapse of a structure.
- The proposed deterioration models incorporate cyclic deterioration controlled by hysteretic energy dissipation as well as deterioration of the backbone curve (strength capping at δ_c/δ_y and a post-capping decrease in strength defined by α_c). This dual deterioration behaviour is equivalent to the two-part damage concept contained in some cumulative damage models such as the Park–Ang model [13]. This model, which was developed specifically for reinforced-concrete components, consists of a linear combination of displacement and energy demands, expressed as follows:

$$\mathrm{DM} = \frac{\delta_{max}}{\delta_{ult}} + \frac{\beta}{F_y \delta_{ult}} \int dHE \tag{8}$$

  where DM is a damage index, δ_{max} is the maximum displacement of the system, δ_{ult} is the monotonic displacement capacity of the system, and β is a structural performance parameter. In concept, the parameters δ_{ult} and β of this cumulative damage model are analogous to δ_c and γ of the proposed deterioration model.
- Figures 8, 10, and 12 show that the reference cyclic hysteretic energy dissipation capacity, $\gamma F_y \delta_y$, is rarely achieved in component tests. Components usually reach zero resistance long before this reference capacity is utilized. This happens because of the presence of strength capping and a negative post-capping tangent stiffness that leads to zero resistance (or a residual strength) even if no cyclic loading is performed. The post-capping strength deterioration and the cyclic strength deterioration are analogous to the phenomena expressed by the two terms of the Park–Ang damage model (Equation (8)).

6. APPLICATION OF HYSTERETIC MODELS TO SEISMIC EVALUATION OF SDOF SYSTEMS

The deterioration models discussed in the previous sections have been employed in an extensive parameter study on the effects of deterioration on the inelastic dynamic response of SDOF systems and MDOF frame structures [14]. Representative results are illustrated in Figures 16 and 17 for a peak-oriented SDOF system subjected to a series of 40 ground motion records. A reference non-deteriorating system is used as well as three systems with various levels of deterioration. The results are not comprehensive, but serve to illustrate the impact that

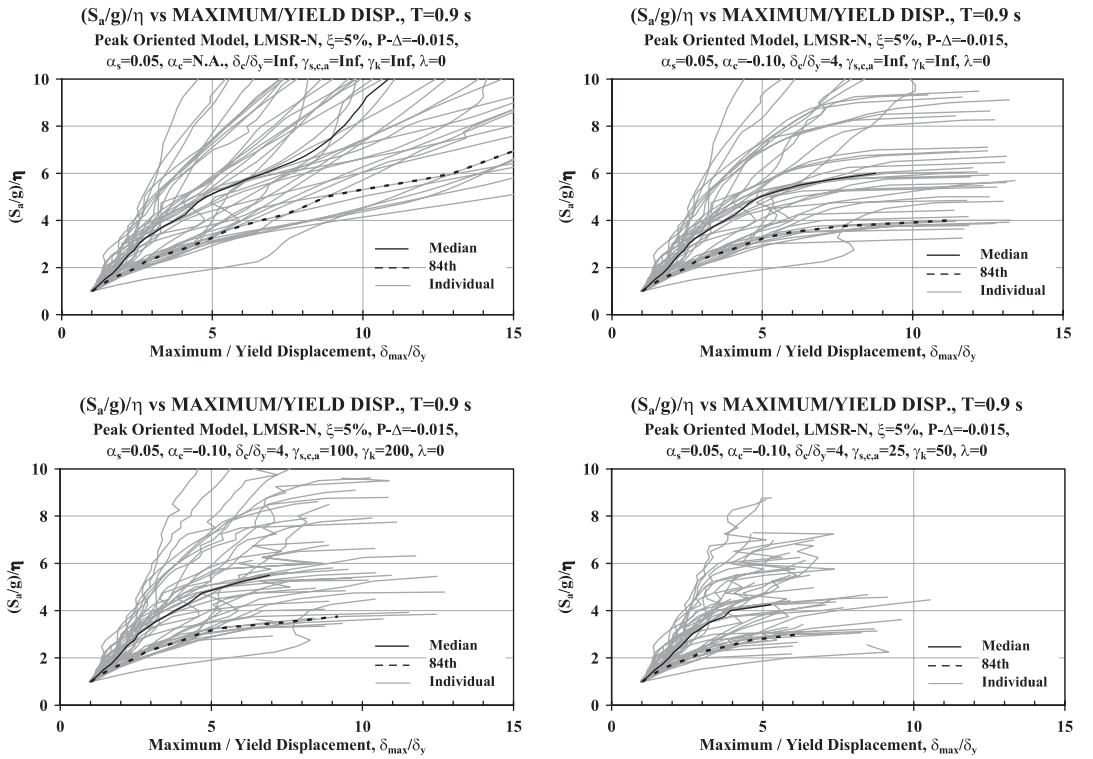

Figure 16. Individual and statistical $(S_a/g)/\eta$–δ_{max}/δ_y relationships for SDOF system with $T = 0.9$ s: (a) non-deteriorating system; (b) $\delta_c/\delta_y = 4$, $\alpha_c = -0.1$, $\gamma_{s,c,k,a} =$ infinite; (c) $\delta_c/\delta_y = 4$, $\alpha_c = -0.1$, $\gamma_{s,c,k,a} = 100$; and (d) $\delta_c/\delta_y = 4$, $\alpha_c = -0.1$, $\gamma_{s,c,k,a} = 25$.

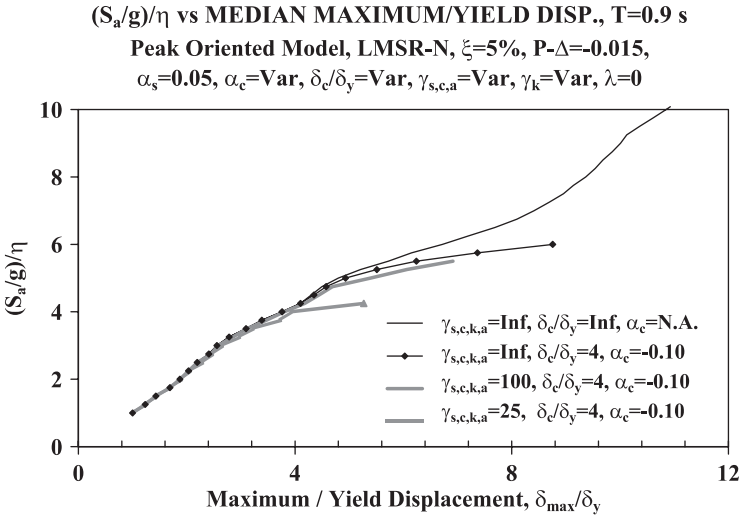

Figure 17. Median $(S_a/g)/\eta$–δ_{max}/δ_y relationships, all cases.

deterioration has on the seismic response, particularly when the structural system approaches the limit state of collapse.

The SDOF system is defined by its period ($T = 0.9$ s), its percentage of critical damping ($\xi = 5\%$), and various strength and deformation parameters. All systems have a yield strength defined by the strength coefficient $\eta = F_y/W$, and 5% strain hardening ($\alpha_s = 0.05$). To simulate $P-\Delta$ effects, an elastic stability coefficient of 0.015 is assumed. By definition, the non-deteriorating system has no post-capping branch and no cyclic deterioration, whereas the three deteriorating systems have a ductility capacity $\delta_c/\delta_y = 4$ and a post-capping stiffness ratio $\alpha_c = K_c/K_e = -0.1$. The variable in the deteriorating systems is the cyclic deterioration parameter $\gamma_{s,c,k,a}$, which is varied from infinite (no cyclic deterioration), to 100 (slow cyclic deterioration), and to 25 (fast cyclic deterioration). In all deterioration cases the exponent in Equation (1) is taken as 1.0.

To obtain statistical response values, the SDOF systems are subjected to a set of 40 ground motions representing seismic excitations from California earthquakes recorded in NEHRP site class D that do not exhibit pulse-type near-fault characteristics (LMSR-N set). The moment magnitude of these records varies from 6.5 to 6.9 and the source-to-site distance ranges from 13 to 40 km. The properties of the ground motion records are described in Medina and Krawinkler [15].

In line with arguments presented in References [14, 15], the maximum dynamic response of SDOF systems is represented in terms of an engineering demand parameter (the ratio δ_{max}/δ_y is used in Figures 16 and 17) versus a parameter called *relative intensity*. The relative intensity is defined as $(S_a/g)/\eta$, with S_a being the ground motion intensity described by the 5% damped linear-elastic spectral acceleration at the period of the SDOF system. The relative intensity is equivalent to the ductility-dependent strength reduction factor, R_μ, if the ground motion intensity (S_a) is kept constant, or it can be viewed as the intensity of the ground motion to which the SDOF system is subjected, if η is assumed to be constant.

To obtain curves of the type shown in Figure 16, a time history analysis is performed by subjecting the SDOF system to a ground motion that is scaled to a specific value of the relative intensity $(S_a/g)/\eta$, and then incrementing the relative intensity to cover the full range of interest. The use of a single set of ground motions implies that the results are applicable for a range of relative intensities over which the ground motion frequency content, and hence, the inelastic structural response, are only weakly dependent on magnitude and distance [15–17]. Collapse is imminent when a very small increment in relative intensity causes a very large increment in displacement of the system, a condition that indicates dynamic instability. In the figures, dynamic instability is indicated when the slope of the $(S_a/g)/\eta$ versus δ_{max}/δ_y curve approaches zero. The largest stable value of $(S_a/g)/\eta$ is denoted as the relative intensity at collapse, or short, the 'collapse capacity' of a specific structure associated with a specific ground motion.

Figure 16 shows individual $(S_a/g)/\eta$ versus δ_{max}/δ_y curves as well as statistical curves representing the median and 84th percentile values of δ_{max}/δ_y, given $(S_a/g)/\eta$, for all four cases. For the non-deteriorating case (Figure 16(a)) all curves continue with a positive slope without ever approaching a state of collapse (because the 5% strain hardening dominates over the 1.5% P–Δ effect). For the three deterioration cases most of the curves for individual ground motions approach a zero slope within the $(S_a/g)/\eta$ range shown, i.e. collapse occurs at $(S_a/g)/\eta$ values less than 10. The collapse capacity and displacement capacity depend on the

rate of deterioration, which is slowest when $\gamma_{s,c,k,a}$, is equal to infinite (no cyclic deterioration) and fastest when $\gamma_{s,c,k,a}$, is equal to 25.

The effect of deterioration is best evaluated from the median curves, which for all four cases are presented in Figure 17. Without deterioration, the system never approaches collapse. If a strength cap is applied (at $\delta_c/\delta_y = 4$), which is followed by a post-capping branch (with $\alpha_c = -0.1$), the median curves deviate from those of the non-deteriorating case to an extent that depends on the rate of cyclic deterioration. For $\gamma_{s,c,k,a}$, equal to infinite, the deviation starts at $\delta_{max}/\delta_y = 4$, which corresponds to the deformation assigned to the strength cap, and strength capping alone leads to collapse at $(S_a/g)/\eta$ of about 6. If the hysteretic energy dissipation capacity is relatively large (i.e. $\gamma_{s,c,k,a} = 100$), which implies a low rate of cyclic deterioration, the effect of cyclic deterioration is small. On the other hand, a value of $\gamma_{s,c,k,a} = 25$, which implies a high rate of cyclic deterioration, leads to an early deviation from the non-deteriorating case and to a considerable decrease in the collapse capacity compared to the case with strength capping but without cyclic deterioration.

The above results demonstrate that modelling of deterioration is not very important at relatively small levels of deformations. However, deterioration becomes an overriding consideration when the structure (in this case represented by a simple SDOF system) approaches collapse. When and to what extent the relationship between the relative intensity and an engineering demand parameter deviates from that of a non-deteriorating system depends on the combination of important system parameters, such as ductility ratio (δ_c/δ_y), post-capping stiffness ratio (α_c), and the energy dissipation capacity of the system, defined by $\gamma_{s,c,k,a}$, which controls cyclic deterioration. The magnitude of the $P-\Delta$ effect also plays an important role. Comprehensive results on the effects of all these parameters for SDOF and MDOF systems are presented in Ibarra [14].

7. CONCLUSIONS

This paper presents the description, calibration and application of relatively simple hysteretic models that incorporate the most important sources of strength and stiffness deterioration. Adequate modelling of deterioration is critical for demand prediction for highly inelastic systems.

The hysteretic models include a post-capping softening branch, residual strength, and cyclic deterioration. Cyclic deterioration permits to trace deterioration as a function of past loading history. The rate of deterioration is defined by the parameter β_i, which depends on the hysteretic energy dissipated in past cycles and on a reference energy dissipation capacity expressed as $\gamma F_y \delta_y$. Four modes of cyclic deterioration can be simulated: basic strength, post-capping strength, unloading stiffness, and accelerated reloading stiffness deterioration. Based on calibrations performed with experimental data from component tests of steel, wood, and reinforced-concrete specimens, it appears that, for a given component, the backbone characteristics and a single parameter ($\gamma_{s,c,k,a}$) that controls *all four modes* of cyclic deterioration are adequate to represent component behaviour *regardless* of the loading history. This conclusion is only preliminary because more work needs to be performed to establish consistent methods for assessing all important deterioration parameters (δ_c/δ_y, α_c, γ'_s, c) for the full range of relevant structural components. Work on this task is in progress.

Results from the seismic evaluation of various SDOF systems demonstrate that strength deterioration becomes a dominant factor when the response of a structure approaches the limit state of collapse. At early stages of inelastic behaviour, both deteriorating and non-deteriorating systems exhibit similar responses. The differences become important when the post-capping stiffness is attained in the response.

In summary, the response of structural systems that undergo large inelastic excursions is controlled by deterioration in assemblies of components. The implementation of a rigorous seismic performance assessment methodology is not complete without models capable of tracking the history of damage until or at least close to collapse and incorporate, in an explicit manner, the effects of deterioration in the seismic response. The deterioration models presented in this paper are intended to assist in accomplishing this objective.

ACKNOWLEDGEMENTS

The authors are grateful to Dr Mohsen Rahnama who developed the early version of the SDOF program SNAP in which the deteriorating models were implemented. Thanks are due to Dr Ashraf Ayoub and Manuel Miranda who contributed to the implementation of the models in SNAP. This research was supported by the NSF sponsored Pacific Earthquake Engineering Research (PEER) Center. The studies of the first author were mainly supported by the Consejo Nacional de Ciencia y Tecnologia (CONACYT) and complemented by funds from PEER. These sources of support are much appreciated.

REFERENCES

1. Clough RW, Johnston SB. Effect of stiffness degradation on earthquake ductility requirements. *Proceedings of Japan Earthquake Engineering Symposium*, Tokyo, Japan, 1966.
2. Takeda T, Sozen MA, Nielson NN. Reinforced concrete response to simulated earthquakes. *ASCE Journal of the Structural Division* 1970; **96**:2557–2573.
3. Wen YK. Method for random vibration of hysteretic systems. *ASCE Journal of the Engineering Mechanics Division* 1976; **112**:249–263.
4. Sivaselvan MV, Reinhorn AM. Hysteretic models for deteriorating inelastic structures. *Journal of Engineering Mechanics* 2000; **126**:633–640.
5. Song J, Pincheira J. Spectral displacement demands of stiffness and strength degrading systems. *Earthquake Spectra* 2000; **16**:817–851.
6. Gatto KS, Uang CM. Effects of loading protocol and rate of loading on woodframe shearwall response. *Seventh U.S. National Conference on Earthquake Engineering*, *EERI*, Oakland, CA, 2002.
7. Rahnama M, Krawinkler H. Effects of soft soil and hysteresis model on seismic demands. *John A. Blume Earthquake Engineering Center Report No. 108*. Department of CEE, Stanford University, 1993.
8. Prakash V, Powell GH, Campbell. DRAIN-2DX: basic program description and user guide. *Report No. UCB/SEMM-1993/17*, University of California, Berkeley, CA, 1993.
9. Mahin SA, Bertero VV. Nonlinear seismic response of a coupled wall system. *ASCE Journal of the Structural Division* 1976; **102**:1759–1980.
10. Uang CM, Yu QS, Gilton CS. Effects of loading history on cyclic performance of steel RBS moment connections. *Proceedings of the 12th WCEE*, Upper Hutt, New Zealand, 2000.
11. Sezen H. Evaluation and testing of existing reinforced concrete building columns. *CE299 Report.* University of California, Berkeley, 2000.
12. Krawinkler H, Parisi F, Ibarra L, Ayoub A, Medina R. Development of a testing protocol for woodframe structures. *CUREE Publication No. W-02*. 2000.
13. Park Y, Ang A. Mechanistic seismic damage model for reinforced concrete. *Journal of Structural Engineering* 1985; **111**:722–739.
14. Ibarra L. Global collapse of frame structures under seismic excitations. *PhD Dissertation*, Department of CEE, Stanford University, 2003.

15. Medina RA, Krawinkler H. Seismic demands for non-deteriorating frame structures and their dependence on ground motions. *John A. Blume Earthquake Engineering Center Report No. 144*. Department of CEE, Stanford University, 2003.
16. Shome N, Cornell A. Probabilistic seismic demand analysis of nonlinear structures. *Report No. RMS-35.* Department of Civil Engineering, Stanford University.
17. Jalayer F. Direct probabilistic seismic analysis: implementing nonlinear dynamic assessments. *PhD Dissertation*, Department of CEE, Stanford University, 2003.

